DOI: 10.1016/j.powtec.2020.09.022

Classification of granular materials via flowability-based clustering with application to bulk feeding

J. Torres-Serra[a,b,*], A. Rodríguez-Ferran[b], E. Romero[b]

[a] *Técnicas Mecánicas Ilerdenses, S.L., Polígono industrial Camí dels Frares, c. Alcarràs, parc. 66, 25190 Lleida, Spain.*
[b] *Department of Civil and Environmental Engineering, Universitat Politècnica de Catalunya, Campus Nord, c. Jordi Girona, 1-3, 08034 Barcelona, Spain.*

Abstract

Feeder selection impacts the performance of bagging machinery throughout its life cycle, and yet it is usually based on qualitative assessments of flowability. We propose a data analysis methodology aimed at verifying the feeder-type classification of powders and grains by cluster analysis on their material properties. Results for a first data set of conventional properties show the granular materials clustered into as many groups as main bulk feeding systems. Mismatch between feeder classes and flowability-based clusters is explained by common industrial practice and incomplete material characterisation. For this reason, we introduce a set of specialised properties measured with the granular flow tester we have recently developed. Results for principal component analysis on a second extended property data set show that similarly flowing granular materials are better detected considering the specialised properties. This research contributes to objectify the decision-making process of bulk feeder selection from the quantitative description of granular flow.

Keywords: classification, cluster analysis, flowability, bulk feeding, granular column collapse

1. Introduction

Selecting the most suitable bulk feeding technique for dosing powders and grains is still a current design issue in the packaging industry. Reliability of the dosing operation is crucial for bagging line manufacturers such as Técnicas Mecánicas Ilerdenses, S.L. (TMI) [1]. Bag-filling machines incorporate various volumetric feeders that transport material batches in gain-in-weight systems [2] downstream towards the filling station. A wide range of granular materials are typically packaged in 5 kg to 50 kg bags and at competitive production rates of the order of $10^2\,\mathrm{kg\,h^{-1}}$ to $10^4\,\mathrm{kg\,h^{-1}}$. Therefore, the chosen feeding system has a direct influence on the finished package quality as well as the overall

*Corresponding author at: Department of Civil and Environmental Engineering, Universitat Politècnica de Catalunya, Campus Nord, c. Jordi Girona, 1-3, 08034 Barcelona, Spain.
Email addresses: joel.torres@upc.edu (J. Torres-Serra), antonio.rodriguez-ferran@upc.edu (A. Rodríguez-Ferran), enrique.romero-morales@upc.edu (E. Romero)

performance of a bagging line. In industrial practice, the anticipation of the handling performance and the particle size distribution of any given material, together with the engineering know-how of the designer, constitute the empirical basis for selecting one of the feeder types in Fig. 1:

- Fluidisation chamber (F) feeders are used for valve bag filling [3] by pneumatic transport of the batches with a pressure vessel.
- Gravity (G) feeders allow free discharge of the granular materials from the supply hopper.
- Screw (S) feeders convey granular materials by positive displacement with one or more augers. Many applications require coupling with vacuum nozzles for deaeration (SD) of the already filled open-mouth bags [3] to densify the granular mass and prepare the package to be closed.
- Belt (T) feeders perform material conveying by positive displacement along a belt.

Fig. 2 shows typical ranges of the median particle size of the powders and bulk solids handled by the main feeding techniques, obtained from available data on the granular materials used in this study. Generally, F-type feeders are used for handling fine-grained materials, as well as S- and SD-fed systems are designed to handle fine-grained, cohesive materials. Moreover, G-type feeders are employed with free-flowing, coarse-grained materials, and T-fed systems are selected for coarse-grained materials including materials prone to jamming or with irregular particle shapes. Other feeding systems are less frequently adopted, including: vibratory tray (V) feeders for positive displacement of fragile, coarse-grained materials; rotary valve (R) feeders for free discharge free-flowing, fine-grained materials; and combined feeding systems, such as GV- and GS-type feeders, especially adapted to handling broad product families. Nevertheless, such a hands-on approach to the feeder selection process is potentially leading the decision maker to ill-informed choices, overly relying on a subjective appreciation of flowability, which is commonly estimated with qualitative *quick tests* [4].

Traditionally, a number of experimental methods using small-scale laboratory tests have been proposed to quantitatively estimate granular flow, including:

- Jenike's flow function, expressing a relationship between yield loci, i.e. between the consolidation stress σ_1 and the unconfined yield strength σ_c, usually measured by means of translational and ring shear testers [5]. Flowability according to Jenike is defined by constant values of the ratio $ff_c = \sigma_1/\sigma_c$, with five flowability levels from not flowing ($ff_c < 1$) to free-flowing ($ff_c > 10$).
- Carr's flowability index, defined as a weighed sum of parameters: two measures of the angle of repose, namely the angles of repose and of spatula; compressibility derived from the aerated and packed bulk densities; and the cohesion and uniformity coefficients obtained by sieving analysis [6]. The resulting point score ranks flowability into seven levels from very, very poor to excellent on a 0–100 scale.

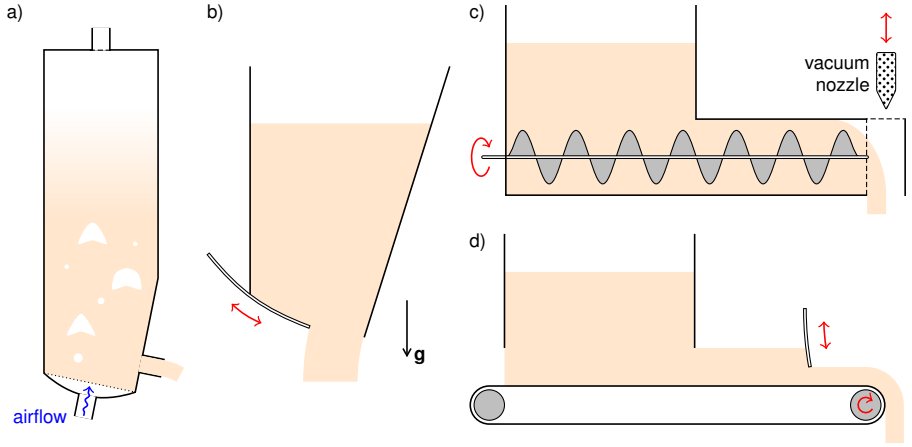

Fig. 1: Schematics of the main bulk feeding techniques: a) F-type feeder with lower inlet for air fluidisation; b) G-type feeder with adjustable gate opening; c) S-type feeder with variable screw rotation, and vacuum nozzle for bag deaeration in SD-fed systems; d) T-type feeder with adjustable belt speed and gate opening.

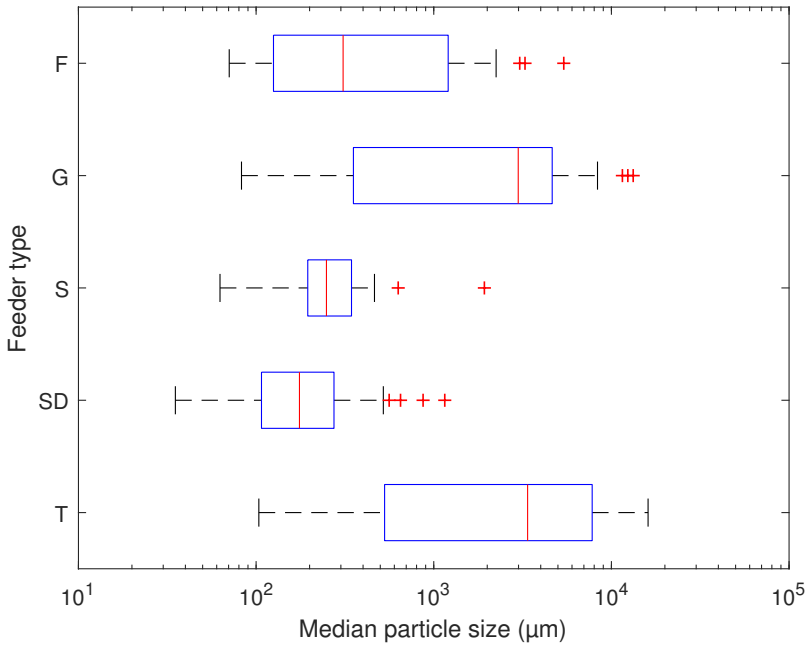

Fig. 2: Box plot of the median particle size of the granular materials studied, grouped by feeder types selected from industrial know-how.

- Geldart's powder classification diagram, described from observation of gas-fluidised beds, considering their mean particle size and particle-fluid density difference for classification [7]. Four fluidisation groups of powders—namely Geldart A (aeratable), B (bubbling), C (cohesive), and D (dense) powders—are identified by their behaviour at the minimum fluidisation and bubbling states.

- More recently, Freeman's flow energies, obtained by dynamic testing of powder samples with a powder rheometer [8]. Flow energy is determined by the resistance to blade rotation coupled with axial motion during powder displacement. Various flowability parameters are defined, such as the basic flowability energy and the specific energy, serving to distinguish powders with similar properties.

These methods offer a fundamental characterisation of powder flow, yet with limited feasibility for coarser granular materials at the standardised lower scales [9]. Alternatively, full-scale pilot plant testing can gauge flow behaviour in actual conditions, although at high costs that make it impractical for routine use [10]. Consequently, we designed, manufactured, and tested an intermediate scale apparatus to describe flow in a granular column collapse set-up [11], which we refer to as the TMI granular flow tester (GFT). This newly patented technology [12] is easily operated and applies to powders and bulk solids in the range of particle sizes from µm to mm.

Fig. 3 illustrates the wide range of granular materials studied in this paper. We observe the variability in two representative material properties: at the particle level, the median particle size in the range of 3.5×10^1 µm to 1.8×10^4 µm, and at the bulk level, the loose bulk density with values between $5.5 \times 10^1\,\mathrm{kg\,m^{-3}}$ and $1.7 \times 10^3\,\mathrm{kg\,m^{-3}}$. Comparing these two properties alone, the granular materials are not distinctively grouped by expected handling performance, and the description of their complex mechanical behaviour is incomplete. The aim of this study is to examine a systematic classification tool to organise the variability in properties describing the flowability of granular materials for practical application in industry.

In recent years, there has been a growing interest in exploiting multivariate analysis methods to predict flow behaviour from experimental measurements [13]. The particle size and shape of pharmaceutical powders have been used to estimate quasi-static flow descriptors, by partial least-squares [14], and using multiple linear regression of relevant parameters selected by principal component analysis (PCA) [15]. Another PCA model has been applied to observe the clustering tendencies and establish the dominant parameters in a pharmaceutical powder database [16]. Moreover, these statistical tools have been used to predict screw feeder performance at powder feeding rates between $0.1\,\mathrm{kg\,h^{-1}}$ and $99.6\,\mathrm{kg\,h^{-1}}$ [17–22]. Particularly, PCA has been reported to enhance the visualisation of pharmaceutical powder clusters with similar flowability [21].

Section 2 presents a data analysis methodology to evaluate the implemented bulk feeding techniques by cluster analysis and to help select the best suited feeder. The flowability of an extensive data set of powders and grains, produced in diverse industrial sectors, is described considering a few conventional material properties. Statistical pre-treatment of the data is based on outlier detection and variable reduction by PCA. In Section 3, we aim at improving the feeder selection associated with the flowability-based clustering. To this end,

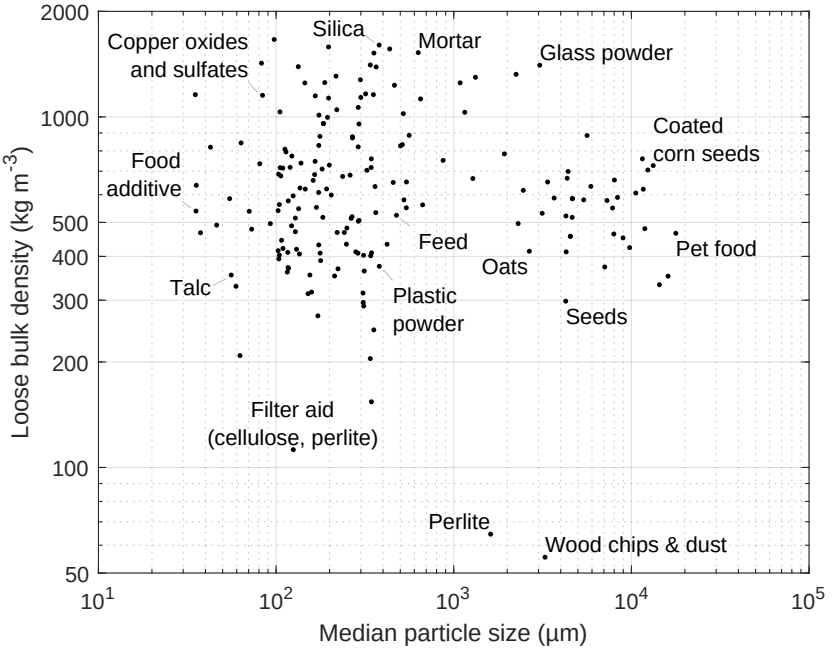

Fig. 3: Range of granular materials studied.

we complement the material characterisation using specialised material properties measured with the GFT, and discuss their contribution to a thorough description of flowability.

2. Data analysis methodology

We gather experimental results by conventional testing of an initial raw data set of 174 granular materials stored in the first data set (DS1) in [23]. We henceforth refer to the rows of DS1 as observations, i.e. the set of information from every granular material, and to the columns of DS1 as variables, containing the different material properties. Table 1 summarises the six available material properties. We denote by ρ_{vib} the bulk density after sample vibration, serving as tapped density in the calculation of the Hausner ratio. We carry out a data treatment scheme for all the granular materials in DS1 to verify their feeder-type classification from industrial know-how against the flowability-based clustering from our analysis of the flow descriptors. For any new material, the workflow consists in updating the following scheme in three main steps, and checking the actually applied technical solution for the closest neighbours. First, we search the raw data set to discard outlying observations. Secondly, we obtain a reduced set of variables via PCA, which explain granular flow in a space of lower dimension. Thirdly, we apply cluster analysis to the low-dimensional space of variables to visualise the clustering tendency in the data. Fig. 4 depicts the data treatment before cluster analysis. We illustrate our methodology using three reference materials, namely O1, O2, and O3, tested as part of the same

Table 1: Conventional material properties in DS1.

Variable type	Symbol	Description	Protocols
State	ρ_b	Loose bulk density ($\mathrm{Mg\,m^{-3}}$)	ASTM D7481 [24]
Mechanical	HR	Hausner ratio (ρ_b/ρ_{vib})	ASTM D4253 [25], USP ⟨1174⟩ [26]
	θ	Angle of repose (°)	Hollow cylinder method [27]
Geometrical (size & shape)	d_{50}	Median particle size (µm)	ASTM C136 [28], ISO 3310-1 [29]
	C_u	Uniformity coefficient (d_{60}/d_{10})	
	C_c	Circularity coefficient (–)	ISO 9276-6 [30]

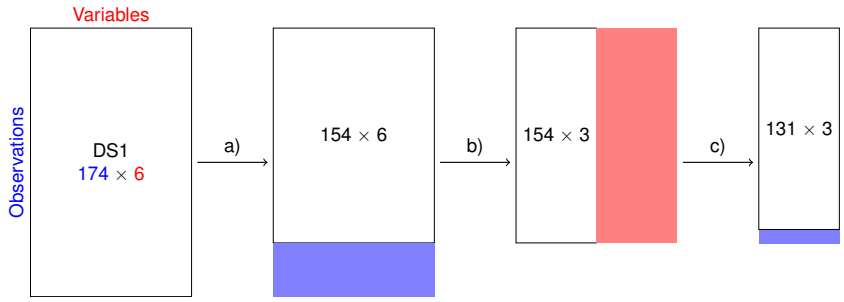

Fig. 4: Data set preparation for cluster analysis, detailed for DS1: a) removal of outlying observations; b) dimensionality reduction via PCA; c) removal of undefined and underpopulated class members.

project for packaging of feed additive powders and bulk solids, which correspond respectively to observations 164, 165, and 166 in DS1.

2.1. Observation selection

Variables showing large dispersion are more likely to include outliers: measurements much smaller or larger than the quantities of interest, which make effectively differentiating between similar observations difficult. We apply a generalised expectation-maximisation algorithm [31] to Gaussian mixture models of the data to find distinct subpopulations in the variables and detect outlying observations. Fig. 5 shows the 174 values of the uniformity coefficient C_u, ranging between 1.0 and 7.8, with $C_u = 3.1$, 3.3, and 3.9 respectively for the reference observations O1, O2, and O3. Applying a three-component mixture model to the C_u data, we note that the values farther from the reference observations are comprised by 'Subpopulation 3', which we remove from further analysis. Analogously, we discard all observations with median particle sizes $d_{50} > 8.1 \times 10^3$ µm, given that the values of interest are between $d_{50} = 1.9 \times 10^2$ µm and 1.9×10^3 µm. We find outliers within the geometrical variables describing the particle size distribution of the samples: outlying observations in d_{50} include coarse-grained materials such as cereal seeds and flakes, hot melt adhesive pearls, and pet food pellets; C_u outliers correspond to well graded mortars, and mixed granular materials forming feed and food additives or chemical compounds. The remaining variables do not present significant outlier subpopulations and so, in total, we keep 154 observations.

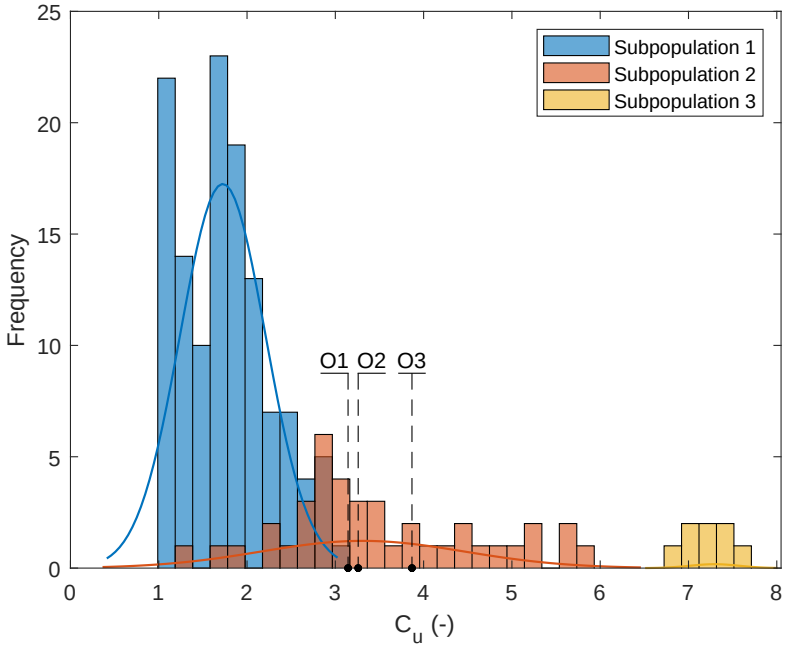

Fig. 5: Detected subpopulations in the C_u data in DS1.

2.2. Variable reduction

To compare the material property values in different scales, we first centre and normalise the original variables. Then, we perform principal component analysis [32] on the standardised variables, to project them into the orthogonal directions carrying the most relevant information from the variables. The projected principal components (PC) explain data variability in such a way that the nth PC explains more data variability from the original data set than the $(n+1)$th PC. We need the first five principal components to capture more than 90 % of the information in the six original variables, as shown by the cumulative explained variance plot in Fig. 6. For data visualisation purposes, we use the reduced set consisting of the first three projected variables, capturing over 75 % of the information in DS1. Fig. 7 shows the coefficients of the principal components, also known as PC loadings: the point areas are proportional to the relative weights of the variables, whereas the contrasting point colours represent the sign patterns of the correlation between variables. The meanings of positive or negative correlation associated with the two colours are interchangeable, since the sign of any given PC is arbitrary [32]. We discuss the data trends in the elements, or PC scores, of the first three principal components, which describe flowability in terms of the conventional material properties:

PC1 Identifies a positive correlation between the mechanical variables, HR and θ, for observations with inversely proportional values of ρ_b, d_{50}, and C_c. Among the analysed materials, fine-grained materials with irregular particle shape show lower bulk density, related to higher compressibility, and steeper angle of repose values. Observation 148 shows the minimum PC1

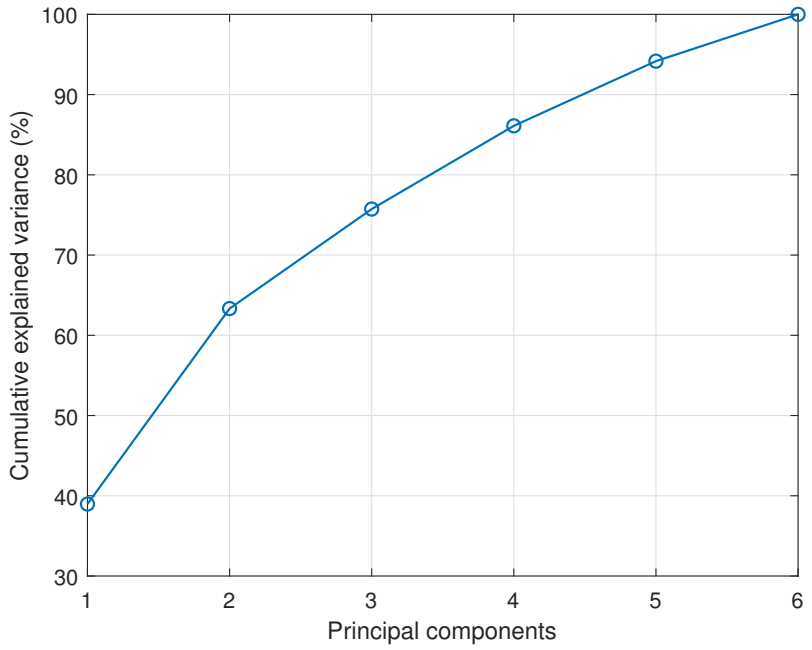

Fig. 6: Cumulative explained variance of the principal components in DS1.

score for a filter aid material, mixing cellulose and perlite powders. Conversely, as in the case of observation O3, lower HR and θ values are shown by denser packings of coarser, rounded particles. The maximum PC1 score is attained by glass beads corresponding to observation 150.

PC2 The geometrical variables describing particle size distribution, d_{50} and C_{u}, are negatively correlated. In turn, fine-grained, well-graded materials show higher bulk density and lower angle of repose values, as we note for O1 and O2, and with minimum PC2 score for a feed powder (observation 51). Oppositely, monodisperse, coarser granular materials present lower bulk density and higher angle of repose, as the pet food pellets (observation 122) having the maximum PC2 score.

PC3 Governed by the state variable ρ_{b}, it indicates a positive correlation between ρ_{b} and θ, both negatively correlated with the C_{u} values. We detect the extreme PC3 scores for observations 90, a high-density micronised zirconium silicate powder, and 139, a low-density sawdust sample.

2.3. Cluster analysis

Granular materials in DS1 are identified by the feeder systems utilised in actual designs. We remove from the analysis those observations with an undefined feeder type or pertaining to classes amounting to less than 5 % of the 154 selected observations. The remaining 131 observations are classified into the predominant bulk feeding techniques: fluidisation chamber (F), gravity (G),

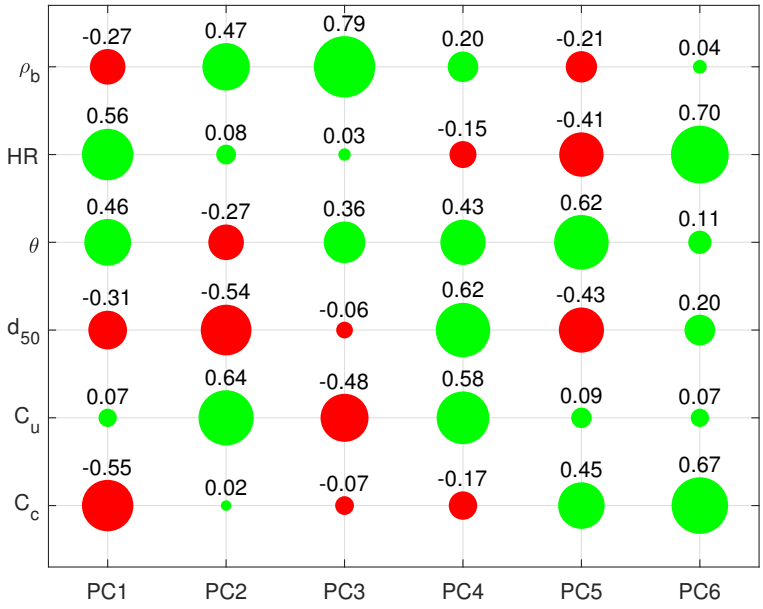

Fig. 7: PC loadings showing the correlation between the original variables and the principal components in DS1.

screw (S) and screw with deaeration (SD), and belt (T). Fig. 8a illustrates the clustering tendency in the labelled observations, as projected into the 3D space maximising their granular flow description. We perform cluster analysis [33] on the reduced variable set to contrast the given feeder-type classification with the resulting flowability-based clustering of the observations. We fix the number of clusters a priori, equal to the five bulk feeding techniques the analysed materials are classified into from industrial know-how. We use the spatial distribution of the feeder-type centroids to initialise the K-means partitioning algorithm implemented in the MATLAB® Statistics and Machine Learning Toolbox™, with the default square Euclidean distance metric. We validate the cluster analysis a posteriori using various statistical criteria, see Appendix A. Fig. 8b shows the grouping of the analysed granular materials into five clusters:

C1 The largest cluster consists of 49 granular materials with centroid near the origin of the PC1-PC2-PC3 space. It is mainly populated by powders, ranging from dairy feed (with up to 13 observations) to polymers, among others, including the feed additive sample O3. Few coarser-grained materials are classified into this cluster, albeit with specific properties contributing to a reduced flowability. Observations 21 and 134 are sepiolite and perlite samples, with low and very low ρ_b respectively, and high C_u in the case of perlite, whereas observation 153 is a rice sample with low C_c.

C2 Its 20 members have the centroid on positive PC2 and PC3, and PC1 values closer to the origin. This cluster shows the minimum pairwise centroid distance with respect to C1, and hence similar materials are expected in

C2. Comparing the reference observations O1 and O2 in C2 with O3 in C1, we find that the samples in C2 show higher ρ_b and lower θ—the negative variable correlation captured by PC2. We note the same data trend between the food additive samples in C2 (observations 101, 103, and 106) and the remaining samples in C1. Moreover, the food additive samples in C2 show higher C_c, a trend explained by PC3 that is also identified in the flour samples distributed between C1 and C2.

C3 With centroid located on values of positive PC1 and PC2, and negative PC3, this cluster comprises 19 granular materials. It includes samples with high ρ_b and C_c values, as in the case of glass beads and crushed glass samples (observations 44, 45, and 71 to 74) or granulated fertilisers (observations 60, 61, 63, 64, and 109 to 113).

C4 The most isolated and least populated cluster, with 15 observations, has its centroid on positive PC1, negative PC2, and values near the origin of PC3. It is composed of samples with large d_{50}, and low C_u and ρ_b, such as plastic pellets, cereal flakes or pet food.

C5 It contains 28 observations with centroid on negative PC1 and PC2, and PC3 values closer to the origin. It is populated by powders and bulk solids mainly characterised by high HR and θ values, as expected from the positive correlation of the mechanical variables revealed by PC1. This cluster includes the maximum observed values of HR and θ, respectively for a filter aid sample (observation 148) and a kaolin powder (observation 30).

Fig. 9 shows the goodness of match between the feeder-type classification and the flowability-based clustering of the analysed granular materials, as typically obtained from the contingency table . We find 59 % of pairs matching with the feeder type SD in cluster C1. This strong interrelation is indicative that SD-fed systems are the most suitable bulk feeding technique for handling granular materials within the C1 borders. However, we observe matching pairs below 50 % for the other clusters and the best-fitted feeder types. We attribute this significant degree of independence between classes and clusters to several factors:

- A single bagging machine is often employed by the end user to pack a product range with distinct mechanical behaviours. This can lead the designer to a suboptimal solution for bulk feeding of the different granular materials. For instance, we consider the reference observations O1, O2, and O3 highlighted in Fig. 8. The implemented screw feeder (S) solution is indeed appropriate for handling O1 and O2, whereas bag deaeration (SD) is also necessary for adequate O3 feeding performance.

- Project requirements are decisive in the design phase of a bagging line. Common industrial practices of the producers may nonetheless interfere with performance-oriented solutions. For example, the usage of valve bags is requested by the producer of resin granules (observation 56), imposing the F-type classification on the only material of this class in cluster C4, see Fig. 8.

- The short number of conventional material properties provide insufficient characterisation of granular flow. In fact, relevant state variables such as

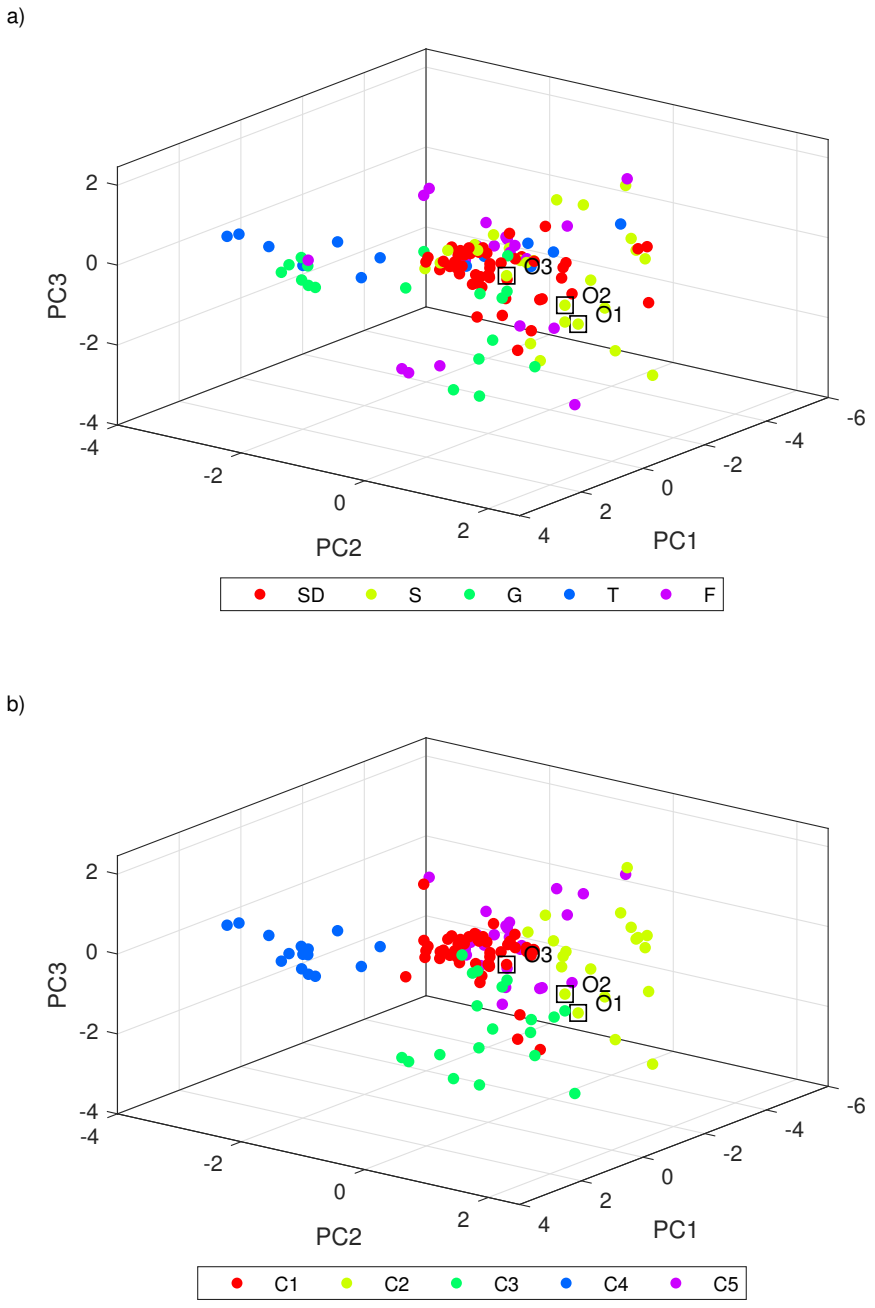

Fig. 8: Projections of DS1 into the first three principal directions. Labels: a) feeder-type classification from industrial know-how; b) flowability-based clustering. Please find the interactive MATLAB® figure files in [23].

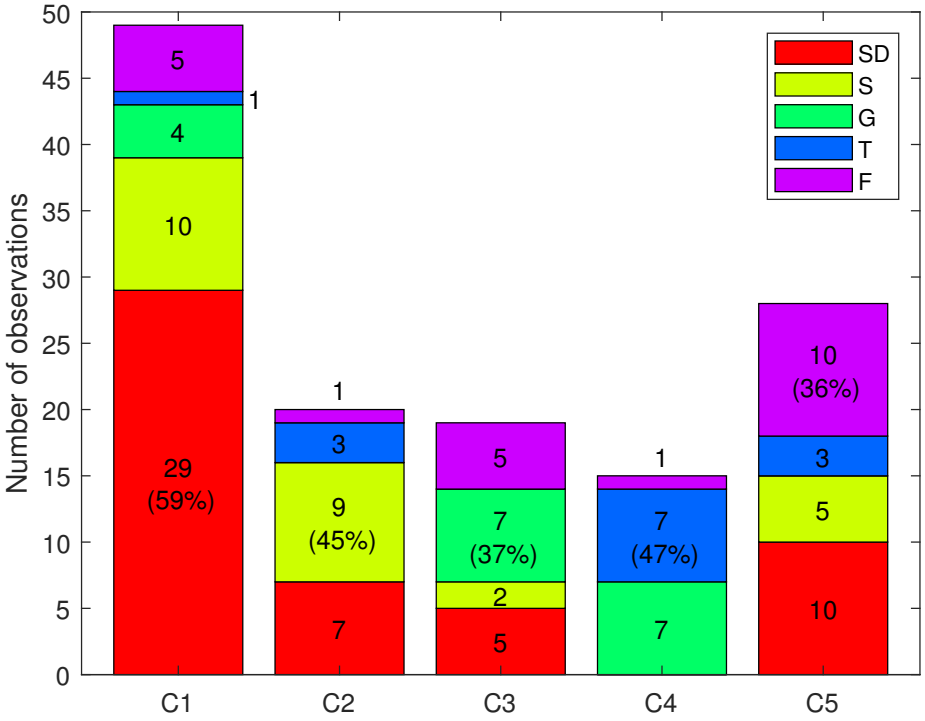

Fig. 9: Frequency distribution of the feeder type classes, and most frequent fractions for each flowability cluster in the reduced DS1.

the particle density and the water content are missing from DS1. Additionally, the available mechanical variables are mostly related to the quasi-static flow regime, typical of stored granular materials at rest.

3. Analysis of an extended property data set

As a strategy to refine the presented data analysis, we recognise the need for gaining insight into the dense and dilute flow regimes occurring in actual handling conditions. Hence, we developed the GFT as an ad hoc experimental set-up [11], composed of a rectangular channel with glass walls, and fully-instrumented as depicted in Fig. 10, allowing us to obtain new material properties from the direct observation of granular column collapse tests [34, 35]. The testing protocol starts by pouring a sample of known mass into the reservoir, enclosed by the gate. Then, the packing state of the granular column is preconditioned with imposed aeration or vacuum conditions. Time zero is set at the beginning of gate lifting, which marks the onset of flow: initially dominated by vertical collapse, and followed by horizontal propagation of the flow front, until the final deposit is formed at run-out.

Table 2 enumerates six test cases covering various initial configurations of the granular column geometry and packing state, for an exhaustive characterisation of any given material. For every test case, we consider at least two representative repetitions to extract the average measurements of the up to 20 specialised material properties listed in Table 3:

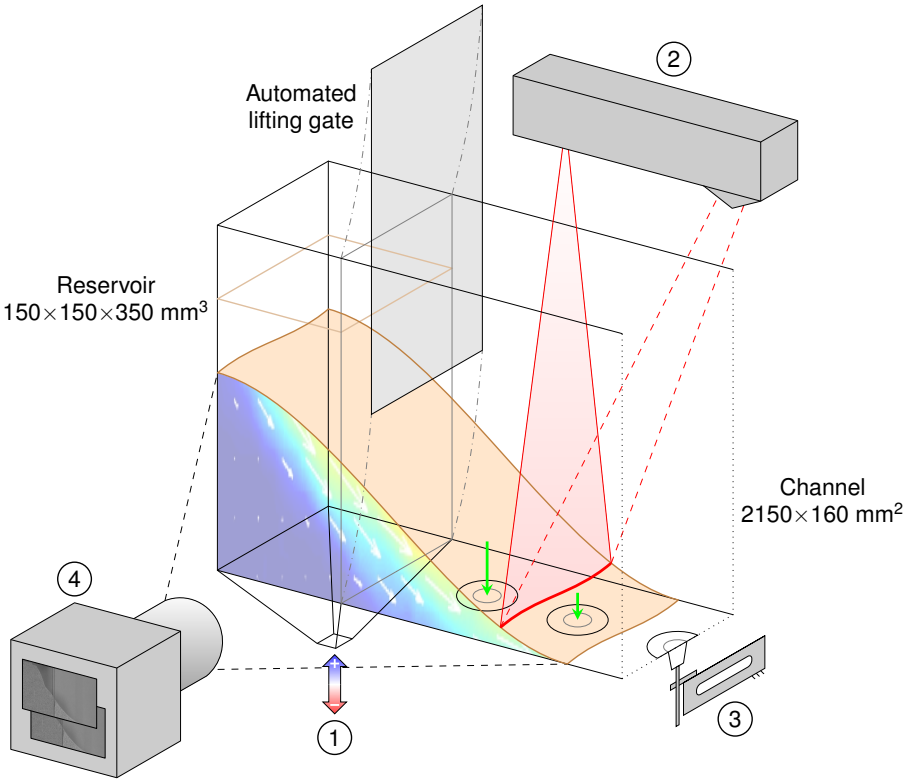

Fig. 10: Annotated diagram of the TMI granular flow tester (GFT) with numbered measuring instruments: 1. reversible pneumatic circuit; 2. 3D laser line profile sensor; 3. membranes and beam load cells; 4. high-speed video camera for particle image velocimetry (PIV) analysis.

Table 2: GFT test case numbering: initial column aspect ratio a against packing state pre-conditioning.

	Poured	Aeration	Vacuum
$a \leq 1$	1	2	3
$a > 1$	4	5	6

- During the pre-conditioning step, the poured random packing state of granular column can be aerated or deaerated with the reversible pneumatic circuit (1). We impose a positive or negative air flow through a porous plate at the reservoir base, reproducing actual bulk handling conditions in fluidisation chamber feeding or bag densification respectively. We estimate the intrinsic air permeability K from the linearised relationship between the air flow and pressure at the column base.

- Fig. 11a represents the variables acquired from the profile sensor (2) surface scans of the initial granular column and the final deposit at rest. We determine the poured bulk density ρ_p using the prismatic volume of the granular column of average poured height h_p. The ratio of the average initial height h_0 to the fixed reservoir length $l_0 = 150\,\mathrm{mm}$ defines the initial column aspect ratio $a \leq 2$. We estimate the angle α by fitting the surface of the final deposit with a sigmoid function, as the arc tangent of the slope at its central point.

- A depositional process takes place during flow front advance, described by a gradual increase of the loads accumulated on the channel surface, until stabilisation. The force distribution is transmitted to a set of beam load cells (LC) triggered at the onset of flow, through silicone membranes embedded along the channel base (3). Granular flow propagation is monitored by a set of transmitters and the basal load profiles are recorded. For $a > 1$, the initial collapse involves a rapid change of momentum of the mobilised mass, resulting in observed load peaks close to the reservoir exit. Fig. 11b shows the fitting parameters for the basal load ramp and peak profiles detected by the first load cell (LC1).

- Using a high-speed video camera (4), we visualise the evolution of the height profiles closer to the glass walls. We derive the incremental kinematic fields from particle image velocimetry (PIV) analysis of the video recordings using the open-source software PIVlab [36]. More details about our PIV approach to the analysis of granular flows can be found in Appendix B. We define the run-out time t_∞ as the first instant at which mobilisation is completed. The evolution of the dominant energy components of the granular system can be seen in Fig. 11c. The total energy E_tot is preserved, and equal to the potential energy E_pot at the onset of flow. The kinetic energy of the system is governed by its translational component $E_\mathrm{kin}^\mathrm{trans}$, found from the combined contributions of the vertical and horizontal components of velocity. A further description of the estimation of kinetic energy from PIV analysis is available in [11].

We build a second data set (DS2) [23] with 11 selected granular materials covering particle sizes of the order of $10^1\,\mu\mathrm{m}$ to $10^4\,\mu\mathrm{m}$ in the range of the

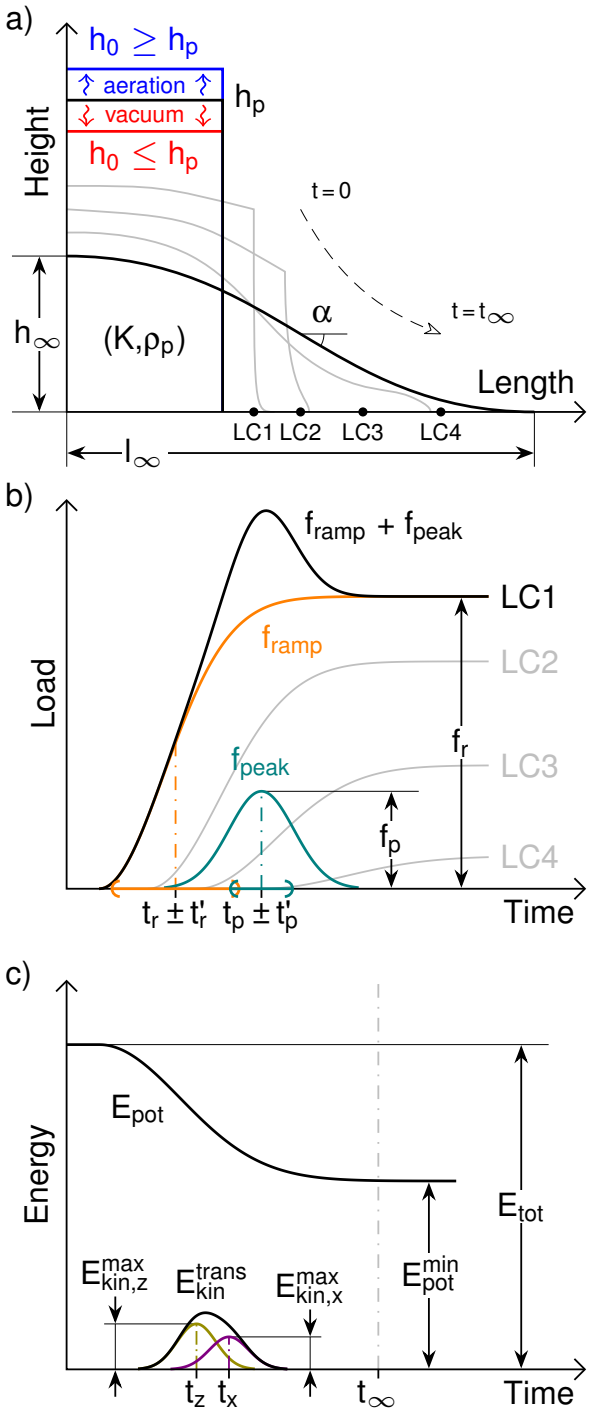

Fig. 11: Graphs of the specialised material properties in Table 3: a) geometry of the granular sample at the poured, initial and final states; b) fitting parameters of the basal load profiles; c) evolution of the system energy components.

Table 3: Specialised material properties in DS2, obtained with the numbered measuring instruments in Fig. 10.

Feature	Phenomenon	Symbol	Description
1	Bed expansion	K	Intrinsic air permeability (m^2)
2	Surface morphology	ρ_p	Poured granular column bulk density ($kg\,m^{-3}$)
		h_p	Poured granular column height (mm)
		h_0	Initial column height after pre-conditioning (mm)
		h_∞	Maximum height of the final deposit (mm)
		l_∞	Run-out length (mm)
		α	Angle of the final deposit (°)
3	Basal load propagation	f_r	Equilibrium load (mN)
		t_r	Ramp time (ms)
		t'_r	Ramp shape (ms)
		f_p	Peak load (mN)
		t_p	Peak time (ms)
		t'_p	Peak shape (ms)
4	Near-wall kinematics	t_∞	Run-out time (s)
		E_{tot}	Total energy of the granular system (J)
		E_{pot}^{min}	Minimum potential energy (J)
		$E_{kin,x}^{max}$	Maximum horizontal kinetic energy (J)
		t_x	Time of $E_{kin,x}^{max}$ (s)
		$E_{kin,z}^{max}$	Maximum vertical kinetic energy (J)
		t_z	Time of $E_{kin,z}^{max}$ (s)

Table 4: Conventional material properties in DS2.

Material	ρ_b ($kg\,m^{-3}$)	HR (–)	d_{50} (µm)	C_u (–)	C_c (–)	w (%)	ρ_s ($kg\,m^{-3}$)	μ_s (–)
Talc	354	1.76	56	1.76	0.35	0.38	2750 [39]	0.4–0.8 [40]
Fertiliser	957	1.08	185	2.01	0.76	1.18	2284 [39]	0.08–0.15 [41]
Feed flour	633	1.21	361	3.78	0.58	9.73	582–739 [42]	0.49–0.69 [42]
Quartz sand	1388	1.10	366	1.67	0.71	0.09	2650	0.58 [43]
Silica	1603	1.25	380	13.1	0.30	0.08	2160–2200	0.49–0.50 [44]
Sugar	833	1.16	514	1.80	0.70	0.28	1576 [45]	0.60–0.71 [46]
Oats	414	1.12	2.66×10^3	2.00	0.63	12.3	950–1397 [47]	0.53–0.62 [47]
LLDPE pellets 1	456	1.05	4.53×10^3	1.19	0.66	0.20	922 [48]	0.28–0.47 [49]
LLDPE pellets 2	585	1.04	4.65×10^3	1.04	0.84	0.09		
Wood pellets	660	1.16	8.02×10^3	1.78	0.60	8.76	1236	0.70–0.84 [9]
Pet food	466	1.10	1.78×10^4	1.12	0.76	9.46	924	0.21–0.47 [50]

granular materials in DS1, as shown in the sieving analysis results in Fig. 12. DS2 includes polydisperse materials, such as the well-graded silica, the study of which is still an open topic in granular mechanics [37]. We take into account 118 specialised variables characterising each observation in DS2, in addition to the 8 conventional material properties presented in Table 4. Compared to the variable set in DS1, the conventional variables in DS2 incorporate the gravimetric water content w, measured according to the standardised procedures in [38], as well as values found in the literature of the particle density ρ_s—otherwise measured by fluid displacement—and the friction coefficient μ_s.

We investigate the variable reduction of DS2, dealing with the data gaps by means of the procedure detailed in [51], which allows us to recover the PCA decomposition of the full data set from the already known material properties. Fig. 13 shows the cumulative explained variance of the projected data set, which carries in the first six principal components over 90 % of the information in DS2. In contrast with the decomposition of DS1, a smaller fraction of the total number of PC is required to capture the same amounts of data variability in

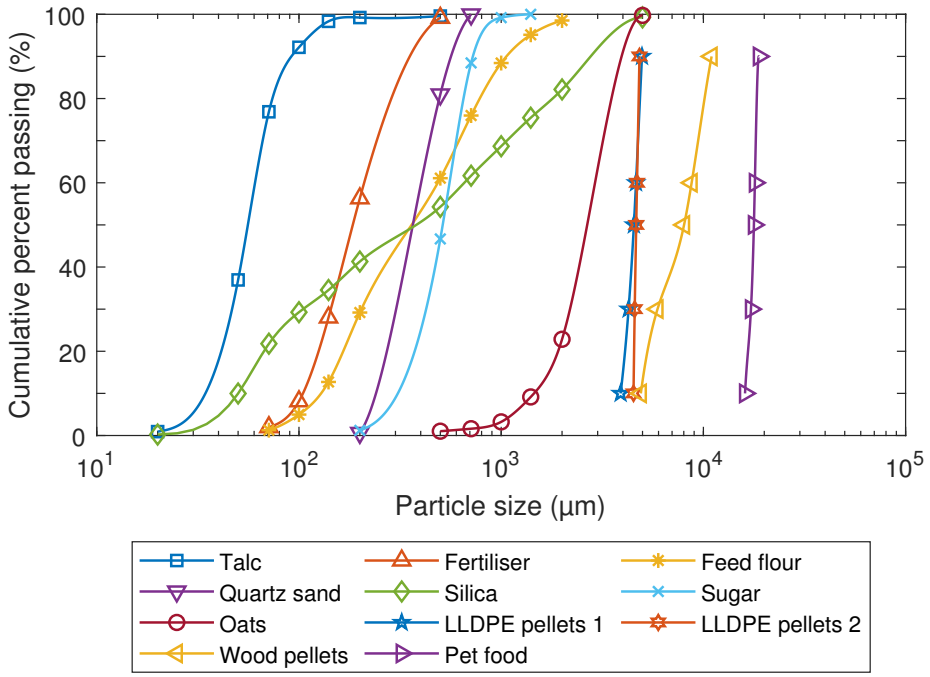

Fig. 12: Particle size distribution curves of the granular materials in DS2.

DS2. We interpret the relative increase of the explained variance as an effect of the comprehensive material characterisation with the GFT. Furthermore, we examine the independence between the conventional and specialised variables in DS2. Fig. 14 shows the poor correlation between the respective PC1-PC2-PC3 of the two variable subsets, thereby confirming that the conventional variables alone cannot explain the new data trends captured by the specialised variables.

We project the observations in DS2 into their first two principal directions, from analysis of the 8 conventional variables in Fig. 15a, and in comparison with the total of 126 conventional and specialised variables in Fig. 15b. For the sake of visualisation, we perform isometric scalings of the observations in Fig. 15 to a unitary average distance. We observe close flowability in both 2D spaces for the two linear low-density polyethylene (LLDPE) pellet samples (labelled P1 and P2), supporting the idea that these materials can be handled by the same bulk feeding technique. Moreover, the detection of similar flow behaviour is enhanced in Fig. 15b for the oats (Q1) and pet food (Q2), which we attribute to an avalanching mechanism noticed during flow propagation in the GFT [11]. This phenomenon is identified by the material properties describing the near-wall kinematics, see Table 3, and related to particle interlocking of irregular-shaped materials—oat flakes and flat ellipsoidal pellets, in this case. Additionally, we consider the silica (R1) and quartz sand (R2), showing similar conventional material properties apart from a much wider particle size distribution in the case of R1, with larger C_u though around similar d_{50}, and less rounded particles, with lower C_c. The estimated flowability of R1 in Fig. 15a is approximately as close to that of R2 as to that of talc (R3). Despite the disparity in conventional

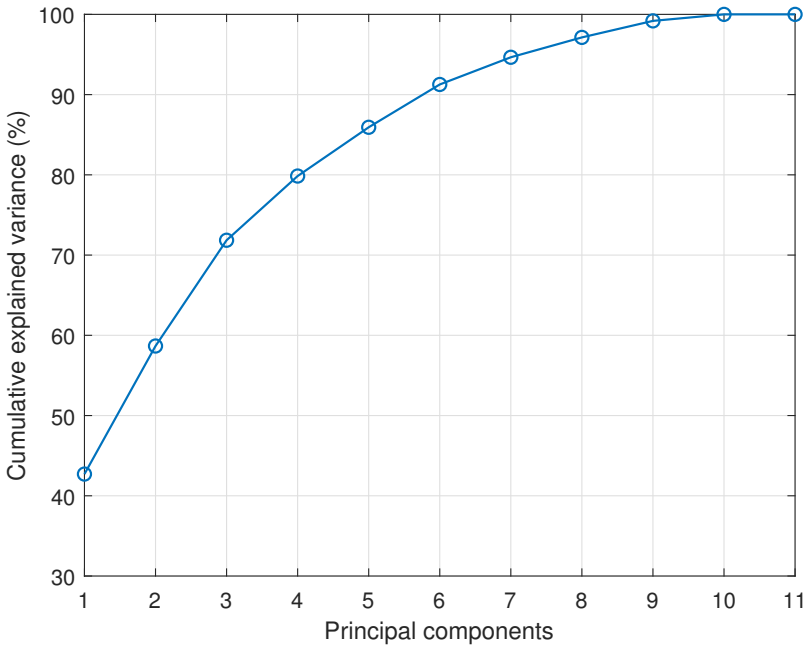

Fig. 13: Cumulative explained variance of the principal components in DS2.

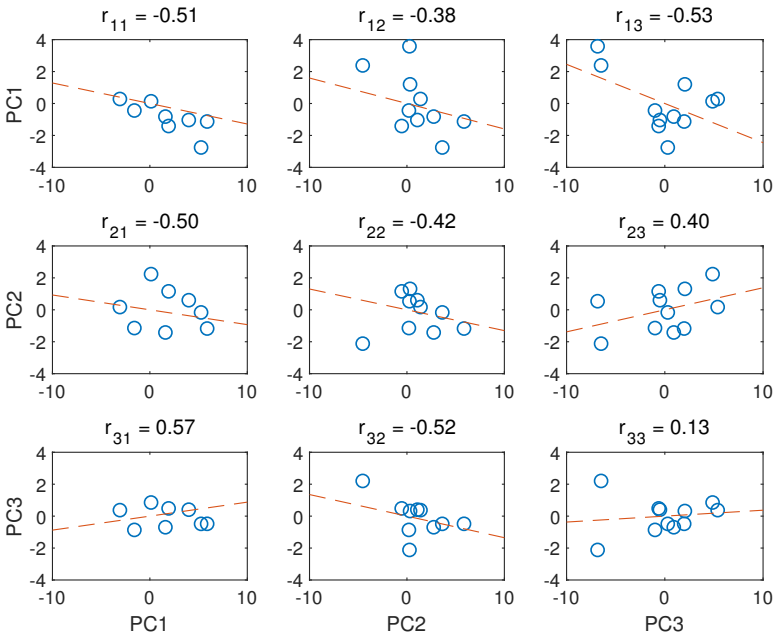

Fig. 14: Correlation between the first three principal components of the conventional (rows i) and specialised (columns j) variable subsets in DS2, annotated with the pairwise Pearson's linear correlation coefficients r_{ij}.

properties, we estimate analogous specialised properties of R1 and R2 by GFT testing, especially the large l_∞, f_p, and $E^{\max}_{\mathrm{kin,x}}$ and $E^{\max}_{\mathrm{kin,z}}$, which we relate with free-flowing materials. As a result, R1 and R2 are relatively closer in Fig. 15a, and their expected flow behaviour is very distant from that of the poorly flowing R3.

These findings indicate that the extended property data set helps in refining the feeder selection by reducing the uncertainty in grouping similar granular materials based on a thorough flowability characterisation. Flowability is a multiphysical, multiscale, coupled phenomenon that has traditionally been approached by selecting a reduced set of material properties partially capturing granular flow behaviour. We discuss variable selection for DS2 in Appendix C, as a trade-off between the interpretability of the data—providing us with a fundamental understanding of the underlying flow mechanisms—and the accuracy of the estimation of flowability—improving the performance of our data analysis methodology for industrial application.

4. Conclusions

We have investigated feeder selection among five bulk feeding techniques used in the packaging industry to handle a wide range of powders and bulk solids from 10^1 µm to 10^4 µm. We have devised a data analysis methodology, applied to the study of DS1, a large data set of 174 granular materials characterised by 6 conventional material properties. We have found that:

- The reduced number of conventional tests, apt for day-to-day industrial practice, allows seeing relevant clustering tendencies in the data. Cluster analysis by K-means partitioning groups similarly flowing materials into an optimum number of clusters equal to the five main bulk feeding techniques.

- As expected, qualitative feeder-type classification based on industrial know-how shows a noticeable disagreement with quantitative flowability-based predictions. The best match, between the SD feeder class and cluster C1, has a 59 % of matching pairs.

New decision-making strategies can be put forward to select the most suitable feeding systems, from the evidence offered by the mismatched materials, as discussed for the reference observation O3. In this way, the end user can be advised about alternative bulk feeding solutions, concerning the recommended type of bag or the number of feeding systems needed to deal with a product range.

We have refined our analysis on the extended property data set DS2, of 11 representative materials characterised by 8 conventional, plus 118 specialised material properties obtained from different test cases with the GFT. Our PCA results show that more data variability in DS2 is explained by fewer principal components with respect to DS1, as well as that there is a lack of correlation between the decomposition of the conventional versus specialised variables in DS2. In sum, the new specialised variables provide a complementary description of granular flow that enhances the detection of similarly flowing materials, such as in the case of observation R1. The GFT is also validated as a powerful tool for the investigation of the flowability of powders and grains.

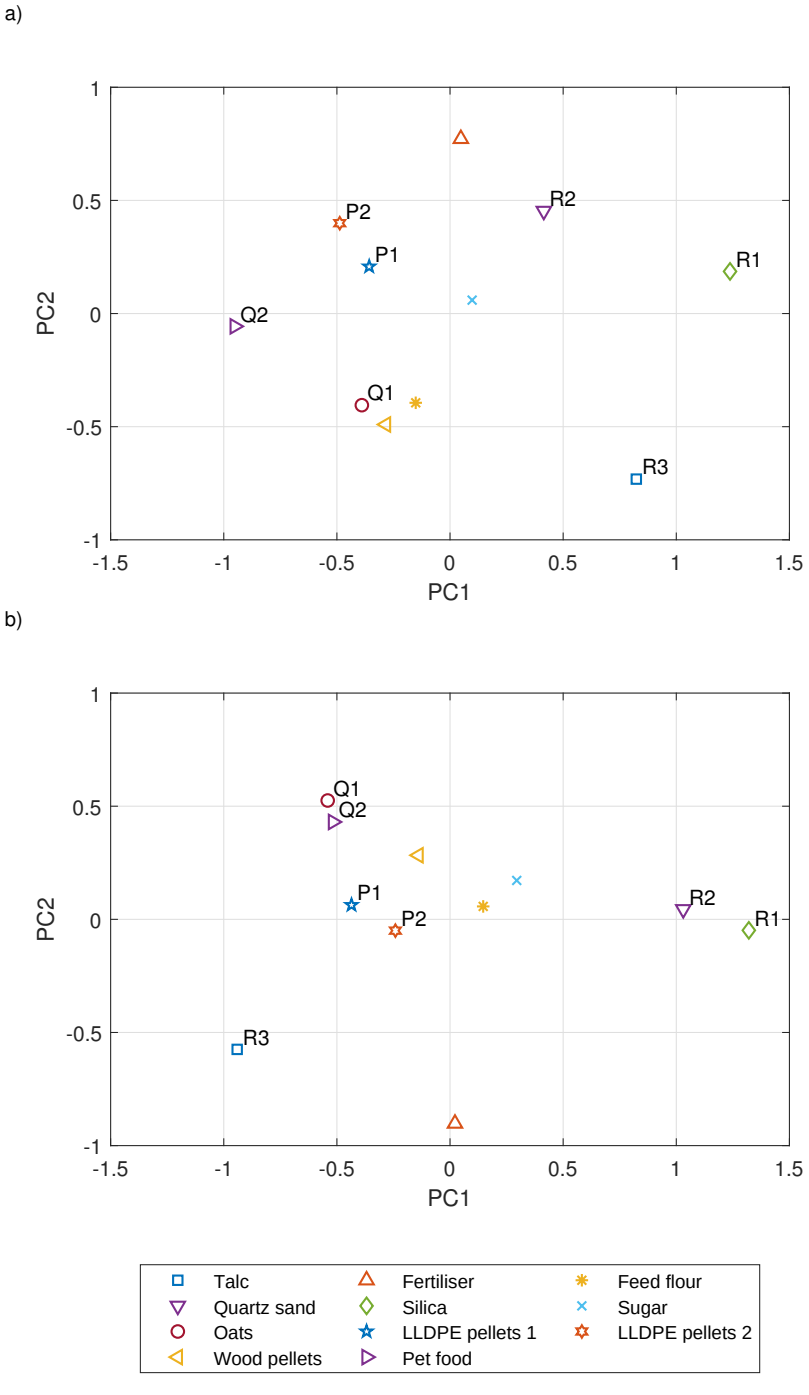

Fig. 15: Scaled projections of DS2 into the first two principal directions, considering: a) the conventional variables; b) the conventional and specialised variables.

In this paper, we have approached flowability as a complex phenomenon through proper statistical treatment of experimental data, in contrast with existing qualitative empirical methods and quantitative testing techniques with limited application. Our findings have implications for improving feeder selection towards an actual flowability-based process, by building robust data sets with a representative variety of granular materials, and fully-characterised with conventional and specialised material properties. Visualisation of the clustering tendencies in the data, by principal component and cluster analysis techniques, groups powders and grains with similar estimated granular flow behaviour. And then, the observed groupings can be verified against uncertain classifications of the adequate bulk feeding techniques, obtained from industrial know-how, for both the analysed granular materials and any new materials being incorporated for classification.

We suggest that further research should address the following topics:

- Verifying the data analysis methodology for larger data sets with extended material properties.
- Validating the clustering through feeder performance assessment by full-scale pilot plant testing.
- Adapting the proposed methodology to selection processes for other bagging machine appliances, such as weighing systems and bag sealing techniques.
- Analysing the influence of the conventional material properties on the specialised flow descriptors, such as the maximum kinetic energy of the granular systems tested with the GFT.
- Extending the specialised characterisation with reverse-calibrated material properties, for instance by discrete element modelling of the GFT set-up to find the mechanical contact parameters.

Acknowledgements

This work was supported by the Industrial Doctorates Plan of the Government of Catalonia (2014 DI 075) and the Centre for the Development of Industrial Technology of the Government of Spain (IDI-20160298). The authors would like to thank Joan Caba, Xavier Arderiu, Josep-Manel Padullés, and Juanjo González at TMI for their valuable contribution to the design and start-up of the TMI granular flow tester.

Appendix A. Cluster analysis validation

We estimate the randomness in DS1 throughout the three analysis steps in Section 2 with the Hopkins statistic [52], averaged over 1000 trials and a sampling window of 10 % of the remaining observations in the data set. Typical values of the Hopkins statistic H range between 0.5 for random data and 1 for well clustered data. The original DS1 has $H = 0.59$, justifying for the data treatment steps before cluster analysis. We calculate $H = 0.90$ after the

Table A.1: Internal validation indices, as summarised in [53], with criteria to determine the optimum number of clusters k^* in each case.

Index	Criterion for k^*
Calinski-Harabasz	Maximum
Davies-Bouldin	Minimum
Silhouette	Maximum
Gap'	Maximum
Hartigan	Smallest k at or below η
Krzanowski-Lai	Maximum

observation selection step, reaching up to $H = 0.98$ after variable reduction, as evidence for the clustering tendency in the projected space. We perform cluster analysis on the first three principal components of the reduced DS1, which retain most of the clusterness of the full decomposition, with an average value of the Hopkins statistic of 0.94.

We evaluate the dispersion of the clustering structure, focusing on the probable number of clusters k in the reduced data set. To this end, we assess the six internal validation indices summarised in [53], each using different criteria to find the optimum number of clusters k^*, see Table A.1. The variety of indices show a discrepancy in k^* found in PC1-PC2-PC3. The number of clusters fixed a priori is only validated by the Hartigan index, defined as the smallest number scoring below the threshold value $\eta = 10$, and which is especially intended to be applied in the K-means algorithm. However, as can be seen in Fig. A.1, all the indices determine the same $k^* = 5$, having discarded as outliers those granular materials with a median particle size $d_{50} > 3\,\mathrm{mm}$. Therefore, we confirm that the most probable number of clusters in the flowability data coincides with the five bulk feeding techniques of interest. Having a different optimum number of clusters $k^* \neq 5$ would not allow us to establish a direct correspondence between classes and clusters. If $k^* < 5$, several feeding techniques might be interchangeable to handle granular materials in the same flowability cluster. Otherwise, if $k^* > 5$, the flowability of different clusters of granular materials within the same feeder-type class might be best fitted by feeding techniques other than the five main ones.

Finally, we assess the similarity between the feeder-type classification and the flowability-based clustering of the reduced DS1 from the observed frequencies of the two groupings, i.e. the contingency table, as depicted in Fig. 9. The Pearson's χ^2 test measures the deviation of the observed frequencies form expectation, with a probability $P(\chi^2 \geq 84) = 1.4 \times 10^{-11}$ on 16 degrees of freedom, a highly significant p-value indicative of the association between the two partitions. We study the goodness of match with different external validation indices [54], also obtained from calculations on the values of the contingency table. From the pairwise comparison of the observations, the Rand index RI is defined between 0 for completely mismatching and 1 for identical clusterings. We find $RI = 0.69$ for the reduced data set, showing a fair agreement between the external classification and the internal clustering. Alternatively, we measure cluster similarity using the amounts of intra- and inter-cluster information, defining the normalised mutual information index $NMI \in [0, 1]$, with lower values for independent clustering scenarios. We compute $NMI = 0.22$,

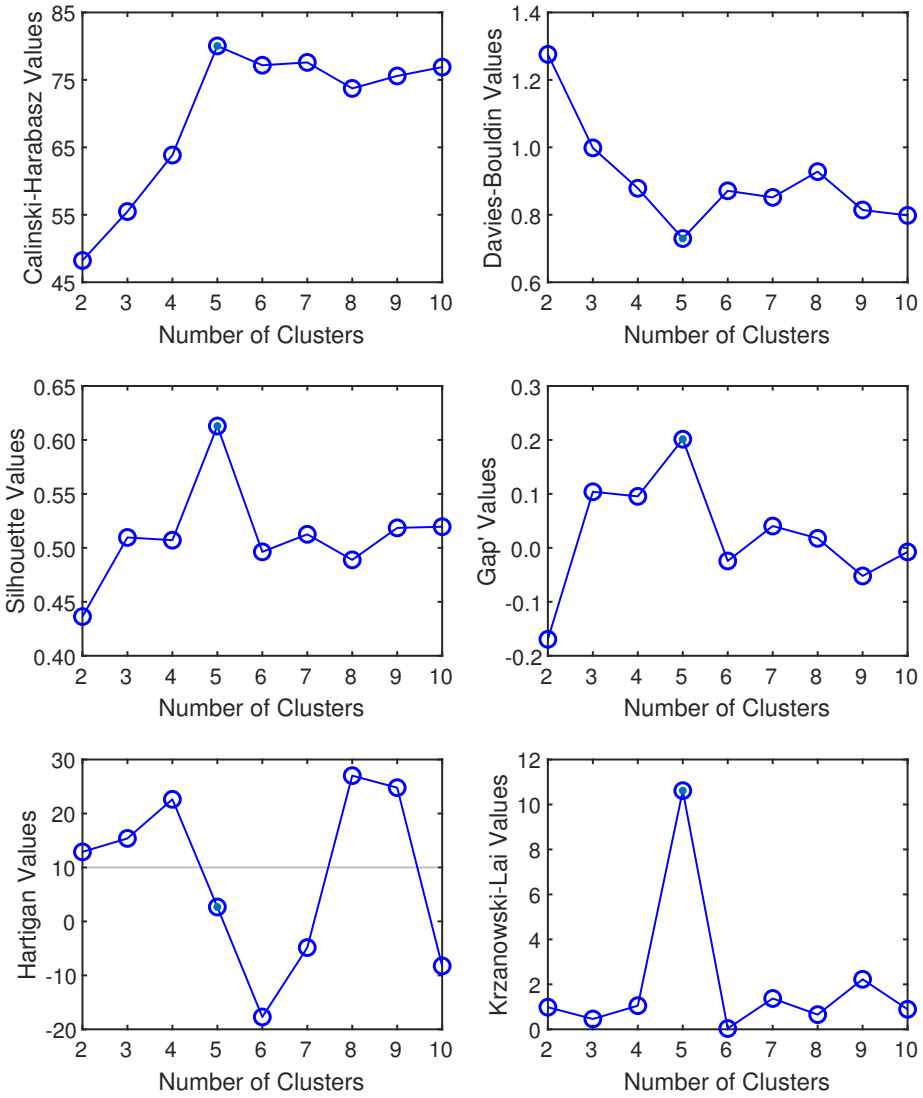

Fig. A.1: Internal validation indices for the reduced DS1, having removed 17 observations with $d_{50} > 3\,\text{mm}$. The Calinski-Harabasz, Davies-Bouldin, and silhouette indices are evaluated with the MATLAB® Statistics and Machine Learning Toolbox™.

which tells us that the feeder-type classification has limited knowledge about the flowability-based clustering. A reasoning for the clustering disagreement is given at the end of Subsection 2.3.

Appendix B. Granular PIV approach

Granular PIV (g-PIV) refers to the application of the PIV technique to the visualisation of granular flows. In the g-PIV, the velocity of particles is measured at a flow boundary illuminated by a lighting system [55], and is mainly used for quasi-two-dimensional set-ups [56], such as unsteady granular column collapse [57, 58], and steady rotating drum and chute flows [59, 60]. The PIV analysis of an image pair, e.g. two consecutive frames from a video recording, recovers the most probable particle displacements by cross-correlation of smaller interrogation areas [36]. We utilise PIVlab version 2.31 [61], with the following default settings: image pre-processing by contrast-limited adaptive histogram equalization (CLAHE), to reduce the uncertainty in locating the correlation peaks, using a window size of 20 pixels (px, $[L^2]$); cross-correlation by fast Fourier transform (FFT) with window deformation, accounting for non-uniform particle motion within the interrogation areas; and a Gaussian 2×3-point fit of the integer displacements of the interrogation areas, to refine the correlation peak location.

We employ a three-pass cross-correlation algorithm with interrogation areas 64×64, 32×32, and 16×16 (px), and 50 % overlap. Multi-pass approaches yield reliable g-PIV estimations depending on the number of particles in the successive interrogation areas, ideally around four and one for the first and last passes, respectively [62]. These optimal conditions are feasible for coarse-grained materials with sufficient inherent texture to detect motion [55], compatible with the experimental lighting conditions and physical resolution of the technique. As a workaround for fine powders and other materials producing low-texture images, we use seeding with tracer particles, also known as markers, which are coarse particles mixed at small mass fractions, of contrasting colour, and similar or lower particle density. As a result, we obtain a mixture of light and dark particles helping to reduce the g-PIV uncertainty [56]. We apply seeding to granular flows of the light-coloured talc, sugar, and the two LLDPE pellet samples in DS2, mixed at 10 %, 5 %, and 10 % mass fractions, respectively. For the talc and sugar, we use blue polystyrene masterbatch granules of median particle size $d_{50} = 2.7\,\mathrm{mm}$, and particle density $\rho_\mathrm{s} = 1.1 \times 10^3\,\mathrm{kg\,m^{-3}}$. Compared GFT experiments of mixed LLDPE pellets and markers are presented in [63].

In addition, we enhance the multi-pass algorithm using different combinations of cross-correlation types and window deformation interpolators, implemented from PIVlab version 2.2 [64]. Correlation quality options include the recommended 'Normal' (circular cross-correlation, linear interpolation), and also 'High' (linear cross-correlation, spline interpolation), which is expected to reduce the measurement errors and improve the robustness of the algorithm for low-quality image pairs. Hence, we apply the 'High' correlation quality to analyse granular flows showing poor g-PIV estimations with the default 'Normal' option, as in the case of the talc, fertiliser, and silica in DS2.

We evaluate the accuracy of the proposed g-PIV approach on semi-synthetic image pairs from GFT recordings of the materials in DS2 with minimum and maximum d_{50}, as shown in Fig. B.1. We select 128×128 px regions of interest

Table B.1: Granular PIV accuracy of the estimated horizontal and vertical displacements, for different multi-pass, enhanced cross-correlation algorithms.

Material	Number of passes	Correlation quality	$\overline{\Delta u_x}$ (px)	$s_{\Delta u_x}$ (px)	$\overline{\Delta u_z}$ (px)	$s_{\Delta u_z}$ (px)
Talc	1	Normal	15.9	0.13	16.0	0.02
		High	15.9	0.08	16.0	0.02
	2	Normal	16.0	1.51	16.0	0.45
		High	15.8	1.79	15.9	0.57
	3	Normal	16.0	0.31	16.0	0.13
		High	16.0	0.36	15.9	0.18
Pet food	1	Normal	15.8	0.15	15.8	0.20
		High	15.8	0.08	15.8	0.09
	2	Normal	15.9	0.09	15.9	0.05
		High	15.9	0.09	15.9	0.03
	3	Normal	16.0	0.06	15.9	0.13
		High	16.0	0.06	15.9	0.13

in original images of granular columns at rest of the talc and pet food samples. We impose an incremental displacement with equal horizontal and vertical components $\Delta u_x = \Delta u_z = 16$ px on Fig. B.1a and Fig. B.1c to obtain the shifted Fig. B.1b and Fig. B.1d, respectively. Table B.1 shows the sample means, $\overline{\Delta u_x}$ and $\overline{\Delta u_z}$, and standard deviations, $s_{\Delta u_x}$ and $s_{\Delta u_z}$, of the estimated Δu_x and Δu_z by one-pass (64×64), two-pass (64×64, 32×32), and three-pass (64×64, 32×32, 16×16) cross-correlation algorithms—interrogation areas in px—with both 'Normal' and 'High' quality enhancements. We discard missing vectors and outliers in the PIVlab analyses with the MATLAB®functions `rmmissing` and `rmoutliers`. We observe accurate $\overline{\Delta u_x}$ and $\overline{\Delta u_z}$ in the case of talc, with $s_{\Delta u_x}$ and $s_{\Delta u_z}$ below 1 px in all the tested configurations except for the two-pass estimation of Δu_x. In the case of pet food, we note increasing accuracy of $\overline{\Delta u_x}$ and $\overline{\Delta u_z}$ with the number of passes, and a greater robustness of the estimations, evidenced by the reduced $s_{\Delta u_x}$ and $s_{\Delta u_z}$. In conclusion, the increasing number of passes improve accuracy, and more clearly for higher-texture images, whereas correlation quality shows a minor impact on the overall acceptable accuracy of the g-PIV estimations. Consequently, we verify our PIV approach to describing the flowability of industrial granular materials, complemented by the measurement redundancy of the fully-instrumented GFT.

Appendix C. Interpretation of PCA in high dimensions

We use PCA to explain flowability by capturing the most data variability in the data sets. Each PC is a linear combination of all the original variables, and thus interpreting the PCA results on the basis of material properties is difficult for data sets with an elevated number of variables, e.g. 126 in the case of DS2. In response to this limitation, simplified PCA approaches have been introduced, see [32], allowing us to try to approximate the complex granular flow behaviour by a subset of the original variables. Sparse PCA (SPCA) is

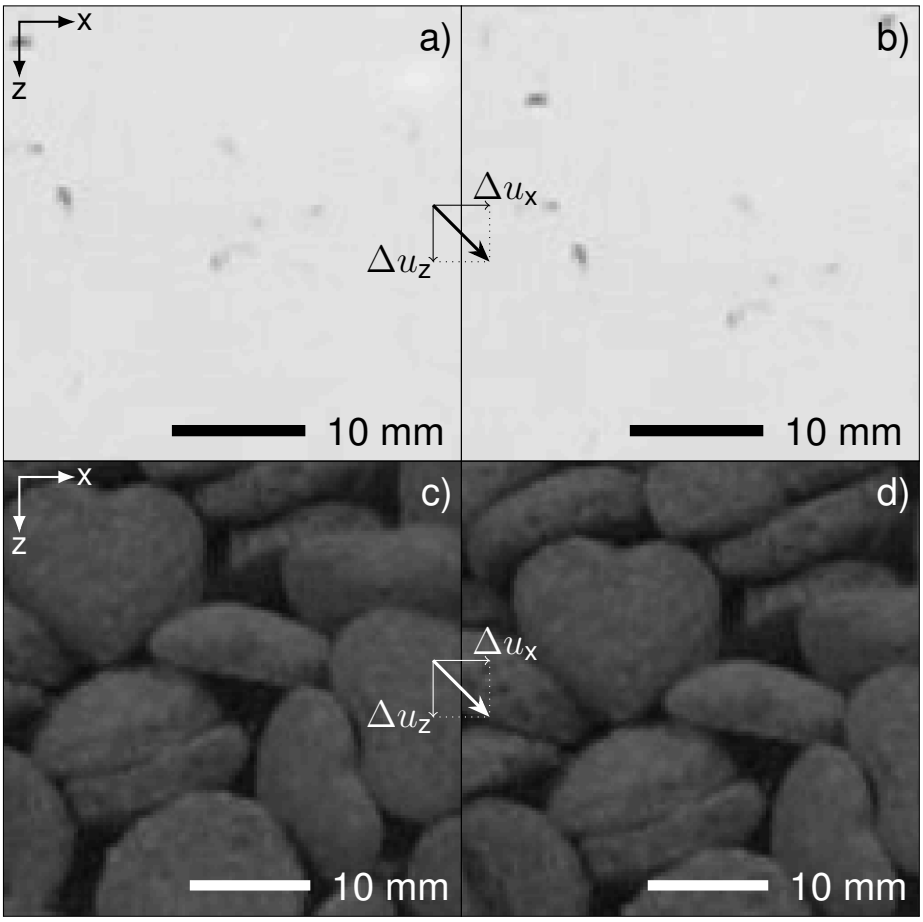

Fig. B.1: Semi-synthetic, 8-bit grayscale image pairs of: a, b) talc with added marker particles; c, d) pet food.

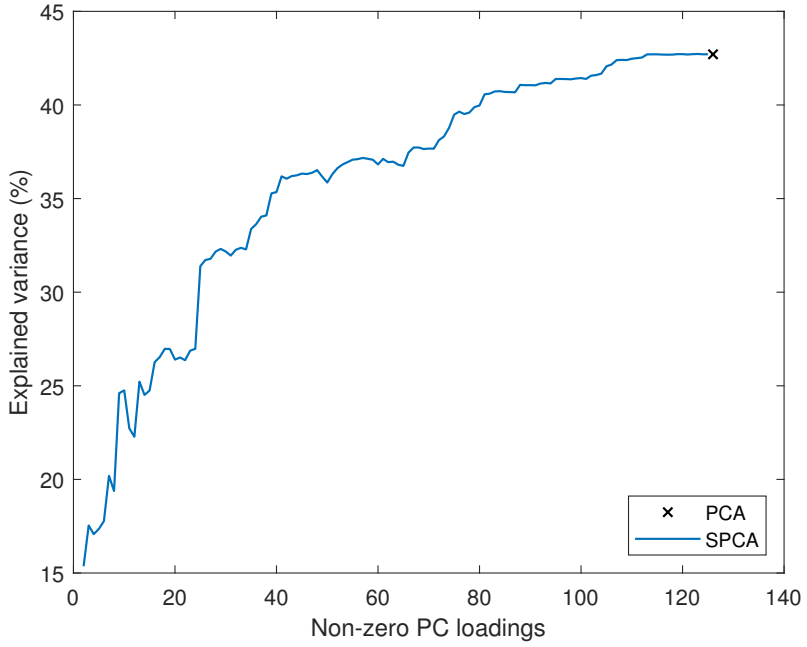

Fig. C.1: Explained variance of the first principal component of DS2 obtained by PCA, and as a function of the number of selected variables by sparse PCA (SPCA).

increasingly used in the study of multiscale phenomena [65], as a technique for selecting the governing coefficients at different scales from traditional PCA decompositions. We examine the variable selection of DS2 using the SPCA algorithm with soft-thresholding regularisation presented in [66], adapted for data sets with a significantly larger number of variables than observations [67], and implemented for MATLAB® in [68].

We observe the decrease of explained variance with increasing sparsity of the PC1 loadings in Fig. C.1. The first principal component obtained by PCA explains 43 % of the variance in DS2, whereas a minimum of 67 non-zero loadings are required to have a reasonable information loss below 5 % of the total variance for the first sparse principal component (SPC1). With a 47 % sparsity, the non-zero PC1 loadings correspond to the conventional variables ρ_b and C_u—with weights 0.17 and 0.05, respectively—and to the specialised variables shown in Fig. C.2. The specialised material properties are described in Table 3, and the test cases are numbered according to Table 2. SPC1 identifies a dominant positive correlation between all the energy components, the poured bulk density, and the ramp and peak loads, across all test cases. Other variables describing surface morphology are also selected, which are negatively correlated with measures of three characteristic times, and air permeability in vacuum conditions. It seems that the granular materials in DS2 are distinctively characterised with the GFT, and that all the different measurements resulting from the sample pre-conditioning and the instrumentation redundancy of the apparatus are necessary as a whole to explain flowability.

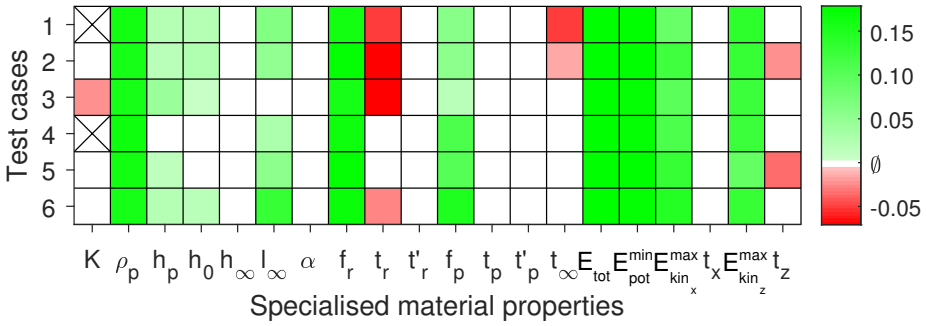

Fig. C.2: PC loadings of the specialised variables in the sparse PC1 (SPC1), explaining 38 % of the total variance in DS2 with 67 non-zero loadings.

In spite of the above findings, SPCA may still be used as a rough estimate of the governing material properties in the data trends revealed by PCA. We approximate the first two principal components of DS2 by selecting a manageable subset of ten original variables in each case. Fig. C.3 shows that SPC1 and SPC2 are dominated by the evolution of the potential energy, and by the initial and final heights, respectively, of the granular systems tested with the GFT. However, compared to the traditional PCA results in Fig. 15b, we note poorer grouping of the materials included in DS2 when projected into SPC1-SPC2, as illustrated in Fig. C.4. The relative positions of the observations in the SPC1-SPC2 space are distorted, affecting the identification of distinctive traits for similarly flowing materials, and even more so for data sets with larger number of observations. Ultimately, we expect the clustering tendency of the data to be affected by variable selection, thereby justifying for the full characterisation of granular materials for practical applications.

References

[1] Técnicas Mecánicas Ilerdenses, S.L., TMI, Ensacado, Paletizado, Protección de cargas y Pesaje (2020).
URL `https://www.tmipal.com/`

[2] J. Marinelli, Choosing a feeder that works in unison with your bin, Powder Bulk Eng. (1996) 43–57.

[3] Center for Chemical Process Safety, Appendix B: Equipment Overview, in: Guidelines for Safe Handling of Powders and Bulk Solids, John Wiley & Sons Ltd, 2004, pp. 577–766. `doi:10.1002/9780470925072.app2`.

[4] L. Bates, Characterisation of Bulk Materials – Industrial Practice, in: D. McGlinchey (Ed.), Characterisation of Bulk Solids, John Wiley & Sons Ltd, 2005, pp. 206–229. `doi:10.1002/9781444305456.ch7`.

[5] D. Schulze, Powders and Bulk Solids, Springer-Verlag Berlin Heidelberg, 2008. `doi:10.1007/978-3-540-73768-1`.

[6] Y. Endo, M. Alonso, An Estimate of Hopper Outlet Size and Slope for Mass Flow from the Flowability Index, Chem. Eng. Res. Des. 80 (6) (2002) 625–630. `doi:10.1205/026387602760312827`.

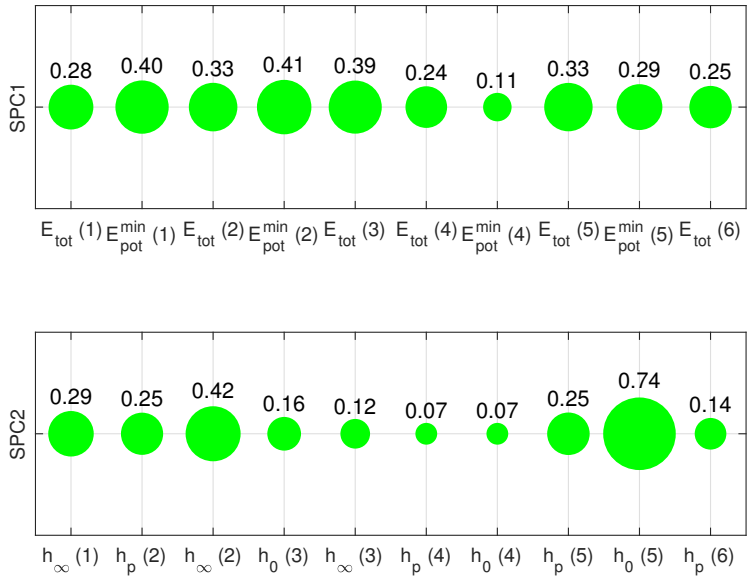

Fig. C.3: Non-zero PC loadings of the SPC1 and SPC2 of DS2, explaining 25 % and 13 % of the total variance in DS2, respectively.

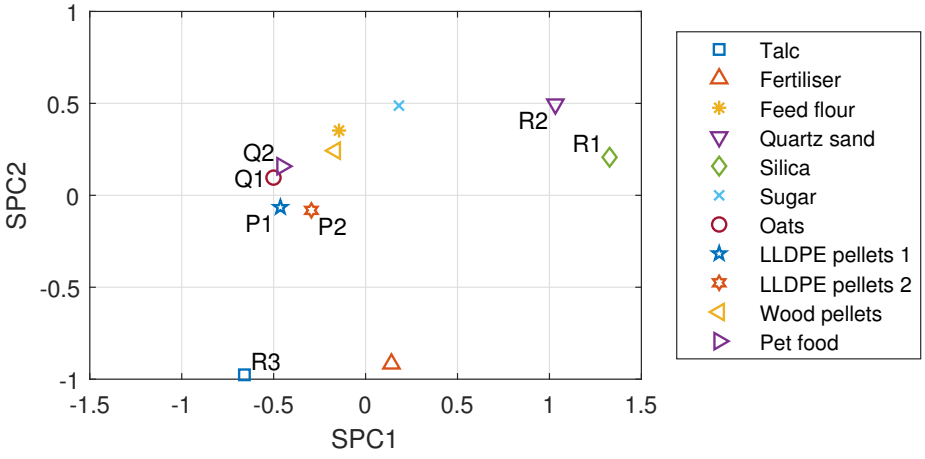

Fig. C.4: Scaled projection of DS2 into SPC1-SPC2 with ten non-zero PC loadings.

[7] D. Geldart, Types of gas fluidization, Powder Technol. 7 (5) (1973) 285–292. doi:10.1016/0032-5910(73)80037-3.

[8] R. Freeman, Measuring the flow properties of consolidated, conditioned and aerated powders — A comparative study using a powder rheometer and a rotational shear cell, Powder Technol. 174 (1) (2007) 25–33. doi:10.1016/j.powtec.2006.10.016.

[9] J.M. Craven, J. Swithenbank, V.N. Sharifi, Investigation into the Flow Properties of Coarse Solid Fuels for Use in Industrial Feed Systems, J. Powder Technol. (2015) 786063doi:10.1155/2015/786063.

[10] J.K. Prescott, R.A. Barnum, On Powder Flowability, Pharm. Technol. 24 (10) (2000) 60+.

[11] J. Torres-Serra, E. Romero, A. Rodríguez-Ferran, A new column collapse apparatus for the characterisation of the flowability of granular materials, Powder Technol. 362 (2020) 559–577. doi:10.1016/j.powtec.2019.11.080.

[12] Técnicas Mecánicas Ilerdenses, S.L., Dispositivo para ensayo de colapso de una columna de material pulverulento o granular, inventors: J. Torres Serra, X. Arderiu Cabau, J.M. Padullés Ribalta, J. Caba Muntada, J.J. González Toledano, E.E. Romero Morales, A. Rodríguez Ferran, Spanish Patent ES2695451B2 (2019).
URL https://patentscope.wipo.int/search/en/detail.jsf?docId=ES235596513

[13] A.J. Rogers, A. Hashemi, M.G. Ierapetritou, Modeling of Particulate Processes for the Continuous Manufacture of Solid-Based Pharmaceutical Dosage Forms, Processes 1 (2) (2013) 67–127. doi:10.3390/pr1020067.

[14] W. Yu, K. Muteki, L. Zhang, G. Kim, Prediction of Bulk Powder Flow Performance Using Comprehensive Particle Size and Particle Shape Distributions, J. Pharm. Sci. 100 (1) (2011) 284–293. doi:10.1002/jps.22254.

[15] Z.A. Worku, D. Kumar, J.V. Gomes, Y. He, B. Glennon, K.A. Ramisetty, Å.C. Rasmuson, P. O'Connell, K.H. Gallagher, T. Woods, N.R. Shastri, A.M. Healy, Modelling and understanding powder flow properties and compactability of selected active pharmaceutical ingredients, excipients and physical mixtures from critical material properties, Int. J. Pharm. 531 (1) (2017) 191–204. doi:10.1016/j.ijpharm.2017.08.063.

[16] B. Van Snick, J. Dhondt, K. Pandelaere, J. Bertels, R. Mertens, D. Klingeleers, G. Di Pretoro, J.P. Remon, C. Vervaet, T. De Beer, V. Vanhoorne, A multivariate raw material property database to facilitate drug product development and enable in-silico design of pharmaceutical dry powder processes, Int. J. Pharm. 549 (1) (2018) 415–435. doi:10.1016/j.ijpharm.2018.08.014.

[17] M. Fonteyne, A. Correia, S. De Plecker, J. Vercruysse, I. Ilić, Q. Zhou, C. Vervaet, J.P. Remon, F. Onofre, V. Bulone, T. De Beer, Impact of microcrystalline cellulose material attributes: A case study on continuous

twin screw granulation, Int. J. Pharm. 478 (2) (2015) 705–717. doi:10.1016/j.ijpharm.2014.11.070.

[18] J. Falk, R.J. Berry, M. Broström, S.H. Larsson, Mass flow and variability in screw feeding of biomass powders — Relations to particle and bulk properties, Powder Technol. 276 (2015) 80–88. doi:10.1016/j.powtec.2015.02.023.

[19] Y. Wang, T. Li, F.J. Muzzio, B.J. Glasser, Predicting feeder performance based on material flow properties, Powder Technol. 308 (2017) 135–148. doi:10.1016/j.powtec.2016.12.010.

[20] N. Bostijn, J. Dhondt, A. Ryckaert, E. Szabó, W. Dhondt, B. Van Snick, V. Vanhoorne, C. Vervaet, T. De Beer, A multivariate approach to predict the volumetric and gravimetric feeding behavior of a low feed rate feeder based on raw material properties, Int. J. Pharm. 557 (2019) 342–353. doi:10.1016/j.ijpharm.2018.12.066.

[21] F. Tahir, J. Palmer, J. Khoo, J. Holman, I.K. Yadav, G. Reynolds, E. Meehan, A. Mitchell, G. Bajwa, Development of feed factor prediction models for loss-in-weight powder feeders, Powder Technol. (2019). doi:https://doi.org/10.1016/j.powtec.2019.09.071.

[22] J. Clayton, Chapter 17 - An Introduction to Powder Characterization, in: A.S. Narang, S.I. Badawy (Eds.), Handbook of Pharmaceutical Wet Granulation, Academic Press, 2019, pp. 569–613. doi:10.1016/B978-0-12-810460-6.00021-X.

[23] J. Torres-Serra, Data for: Classification of granular materials via flowability-based clustering with application to bulk feeding, Mendeley Data, version V1 (2020). doi:10.17632/sxg3hg3txw.1.

[24] ASTM D7481-18, Standard Test Methods for Determining Loose and Tapped Bulk Densities of Powders using a Graduated Cylinder, ASTM International (2018). doi:10.1520/D7481-18.

[25] ASTM D4253-16, Standard Test Methods for Maximum Index Density and Unit Weight of Soils Using a Vibratory Table, ASTM International (2016). doi:10.1520/D4253-16.

[26] US Pharmacopeial Convention, ⟨1174⟩ Powder Flow, in: USP 35–NF 30, 2012.

[27] H.M.B. Al-Hashemi, O.S.B. Al-Amoudi, A review on the angle of repose of granular materials, Powder Technol. 330 (2018) 397–417. doi:10.1016/j.powtec.2018.02.003.

[28] ASTM C136 / C136M-14, Standard Test Method for Sieve Analysis of Fine and Coarse Aggregates, ASTM International (2014). doi:10.1520/C0136_C0136M-14.

[29] ISO 3310-1, Test sieves – Technical requirements and testing – Part 1: Test sieves of metal wire cloth (2016).

[30] ISO 9276-6, Representation of results of particle size analysis – Part 6: Descriptive and quantitative representation of particle shape and morphology (2008).

[31] K.R. Koch, Robust estimation by expectation maximization algorithm, J. Geodesy 87 (2) (2013) 107–116. doi:10.1007/s00190-012-0582-3.

[32] I.T. Jolliffe, J. Cadima, Principal component analysis: a review and recent developments, Philos. Trans. R. Soc. A-Math. Phys. Eng. Sci. 374 (2065) (2016) 20150202. doi:10.1098/rsta.2015.0202.

[33] A.K. Jain, Data clustering: 50 years beyond K-means, Pattern Recognit. Lett. 31 (8) (2010) 651–666. doi:10.1016/j.patrec.2009.09.011.

[34] G. Lube, H.E. Huppert, R.S.J. Sparks, M.A. Hallworth, Axisymmetric collapses of granular columns, J. Fluid Mech. 508 (2004) 175—199. doi:10.1017/S0022112004009036.

[35] E. Lajeunesse, A. Mangeney-Castelnau, J.P. Vilotte, Spreading of a granular mass on a horizontal plane, Phys. Fluids 16 (7) (2004) 2371–2381. doi:10.1063/1.1736611.

[36] W. Thielicke, E.J. Stamhuis, PIVlab – Towards User-friendly, Affordable and Accurate Digital Particle Image Velocimetry in MATLAB, J. Open Res. Softw. 2 (1) (2014) e30. doi:10.5334/jors.bl.

[37] M. Cabrera, N. Estrada, Granular column collapse: Analysis of grain-size effects, Phys. Rev. E 99 (1) (2019) 012905. doi:10.1103/PhysRevE.99.012905.

[38] ASTM D4959-16, Standard Test Method for Determination of Water Content of Soil By Direct Heating, ASTM International (2016). doi:10.1520/D4959-16.

[39] S. Kim, J. Chen, T. Cheng, A. Gindulyte, J. He, S. He, Q. Li, B.A. Shoemaker, P.A. Thiessen, B. Yu, L. Zaslavsky, J. Zhang, E.E. Bolton, PubChem 2019 update: improved access to chemical data, Nucleic Acids Res. 47 (D1) (2018) D1102–D1109. doi:10.1093/nar/gky1033.

[40] X. Chen, A.S. Elwood Madden, Z. Reches, The frictional strength of talc gouge in high-velocity shear experiments, J. Geophys. Res.-Solid Earth 122 (5) (2017) 3661–3676. doi:10.1002/2016JB013676.

[41] T. Oishi, M. Goto, A. Kasahara, M. Tosa, Low frictional copper oxide film prepared with sodium hydroxide solution, Surf. Interface Anal. 36 (8) (2004) 1259–1261. doi:10.1002/sia.1889.

[42] M. Molenda, M.D. Montross, J. Horabik, I.J. Ross, Mechanical Properties of Corn and Soybean Meal, Trans. ASAE 45 (6) (2002) 1929–1936. doi:10.13031/2013.11408.

[43] G.C. Cho, J. Dodds, J.C. Santamarina, Particle Shape Effects on Packing Density, Stiffness, and Strength: Natural and Crushed Sands, J. Geotech. Geoenviron. Eng. 132 (5) (2006) 591–602. doi:10.1061/(ASCE)1090-0241(2006)132:5(591).

[44] K. Kawai, H. Sakuma, I. Katayama, K. Tamura, Frictional characteristics of single and polycrystalline muscovite and influence of fluid chemistry, J. Geophys. Res.-Solid Earth 120 (9) (2015) 6209–6218. doi:10.1002/2015JB012286.

[45] L.C. dos Santos, R. Condotta, M.C. Ferreira, Flow properties of coarse and fine sugar powders, J. Food Process Eng. 41 (2) (2018) e12648. doi:10.1111/jfpe.12648.

[46] A. Ramírez, M. Moya, F. Ayuga, Determination of the Mechanical Properties of Powdered Agricultural Products and Sugar, Part. Part. Syst. Charact. 26 (4) (2009) 220–230. doi:10.1002/ppsc.200800016.

[47] J.M. Boac, M.E. Casada, R.G. Maghirang, J.P. Harner III, Material and Interaction Properties of Selected Grains and Oilseeds for Modeling Discrete Particles, Trans. ASABE 53 (4) (2010) 1201–1216. doi:10.13031/2013.32577.

[48] M.A. Spalding, D.E. Kirkpatrick, K.S. Hyun, Coefficients of dynamic friction for low density polyethylene, Polym. Eng. Sci. 33 (7) (1993) 423–430. doi:10.1002/pen.760330708.

[49] A. Akinci, S. Yilmaz, U. Sen, Wear Behavior of Basalt Filled Low Density Polyethylene Composites, Appl. Compos. Mater. 19 (3) (2012) 499–511. doi:10.1007/s10443-011-9208-9.

[50] N. White, D. Jayas, Physical properties of canola and sunflower meal pellets, Can. Biosyst. Eng. 43 (2001) 3.49–3.52.
URL http://www.csbe-scgab.ca/docs/journal/43/c0124.pdf

[51] R. Everson, L. Sirovich, Karhunen–Loève procedure for gappy data, J. Opt. Soc. Am. A 12 (8) (1995) 1657–1664. doi:10.1364/JOSAA.12.001657.

[52] A. Banerjee, R. Davé, Validating clusters using the Hopkins statistic, in: 2004 IEEE International Conference on Fuzzy Systems (IEEE Cat. No.04CH37542), Vol. 1, 2004, pp. 149–153. doi:10.1109/FUZZY.2004.1375706.

[53] A. Albalate, D. Suendermann, A Combination Approach to Cluster Validation Based on Statistical Quantiles, in: 2009 International Joint Conference on Bioinformatics, Systems Biology and Intelligent Computing, 2009, pp. 549–555. doi:10.1109/IJCBS.2009.116.

[54] A.J. Gates, I.B. Wood, W.P. Hetrick, Y.Y. Ahn, Element-centric clustering comparison unifies overlaps and hierarchy, Sci. Rep. 9 (2019) 8574. doi:10.1038/s41598-019-44892-y.

[55] W. Eckart, J.M.N.T. Gray, K. Hutter, Particle Image Velocimetry (PIV) for Granular Avalanches on Inclined Planes, in: K. Hutter, N. Kirchner (Eds.), Lecture Notes in Applied and Computational Mechanics, Vol. 11, Springer, Berlin, Heidelberg, 2003, pp. 195–218. doi:10.1007/978-3-540-36565-5_6.

[56] R.M. Lueptow, A. Akonur, T. Shinbrot, PIV for granular flows, Exp. Fluids 28 (2) (2000) 183–186. doi:10.1007/s003480050023.

[57] G. Lube, H.E. Huppert, R.S.J. Sparks, A. Freundt, Collapses of two-dimensional granular columns, Phys. Rev. E 72 (4) (2005) 041301. doi:10.1103/PhysRevE.72.041301.

[58] E. Lajeunesse, J.B. Monnier, G.M. Homsy, Granular slumping on a horizontal surface, Phys. Fluids 17 (10) (2005) 103302. doi:10.1063/1.2087687.

[59] D. Gollin, W. Brevis, E.T. Bowman, P. Shepley, Performance of PIV and PTV for granular flow measurements, Granul. Matter 19 (3) (2017) 42. doi:10.1007/s10035-017-0730-9.

[60] L. Sarno, A. Carravetta, Y.C. Tai, R. Martino, M.N. Papa, C.Y. Kuo, Measuring the velocity fields of granular flows – Employment of a multi-pass two-dimensional particle image velocimetry (2D-PIV) approach, Adv. Powder Technol. 29 (12) (2018) 3107–3123. doi:10.1016/j.apt.2018.08.014.

[61] W. Thielicke, PIVlab - particle image velocimetry (PIV) tool, MATLAB Central File Exchange version 2.31 (2019).
URL https://www.mathworks.com/matlabcentral/fileexchange/27659-pivlab-particle-image-velocimetry-piv-tool

[62] L. Sarno, Y.C. Tai, A. Carravetta, R. Martino, M.N. Papa, C.Y. Kuo, Challenges and improvements in applying a particle image velocimetry (PIV) approach to granular flows, J. Phys.: Conf. Ser. 1249 (2019) 012011. doi:10.1088/1742-6596/1249/1/012011.

[63] J. Torres-Serra, E. Romero, A. Rodríguez-Ferran, A New Granular Column Collapse Device to Characterise Flowability of Bulk Materials, Proceedings 2 (8) (2018) 488. doi:10.3390/ICEM18-05389.

[64] W. Thielicke, Evaluation of the new PIVlab (v2.2) settings (2019).
URL https://pivlab.blogspot.com/2019/09/evaluation-of-new-pivlab-v21-settings.html

[65] N.B. Erichson, P. Zheng, K. Manohar, S.L. Brunton, J.N. Kutz, A.Y. Aravkin, Sparse Principal Component Analysis via Variable Projection, SIAM J. Appl. Math. 80 (2) (2020) 977–1002. doi:10.1137/18M1211350.

[66] H. Zou, T. Hastie, R. Tibshirani, Sparse Principal Component Analysis, J. Comput. Graph. Stat. 15 (2) (2006) 265–286. doi:10.1198/106186006X113430.

[67] H. Zou, T. Hastie, elasticnet: Elastic-Net for Sparse Estimation and Sparse PCA, R package version 1.3 (2020).
URL https://CRAN.R-project.org/package=elasticnet

[68] M. Ali, Sparse Kernel Principal Component analysis, MATLAB Central File Exchange version 1.0 (2016).
URL https://www.mathworks.com/matlabcentral/fileexchange/58939-sparse-kernel-principal-component-analysis